Topological Studies of Bimodal Networks

P. R. von Lockette and E. M. Arruda*

*Mechanical Engineering and Applied Mechanics, Macromolecular Science and Engineering,
The University of Michigan Ann Arbor, Michigan 48109-2125*

ABSTRACT: A new cross-linking algorithm, NETSIM, is described which enables the study of continuously spatially distributed (off-lattice) polymer networks and reveals some topological features possibly associated with the enhanced mechanical properties seen in certain bimodal elastomer networks. These features are identified based on trends in their occurrence at various mole fraction and molecular weight combinations and comparison with data found in the literature. A length scale, the *linear cross-link spacing*, is defined which is associated with these features, to characterize optimal bimodal mixture combinations. NETSIM is unique among cross-linking algorithms in that it employs nearest-neighbor periodic boundary conditions to eliminate edge effects and reduce the necessary computational size from over 10000 primary chains to roughly 1000. Computational size reduction eliminates the need for subdivision of the cell, a possible source of bias in results reported in previous research. This work also offers, for the first time, computationally determined gel fraction and extent of reaction calculations for various bimodal mixture compositions. For verification, NETSIM results on unimodal systems are compared to previous unimodal simulations with good agreement.

1. Introduction

Elastomers are important engineering materials due to their ability to recover completely from large deformations and to exhibit a repeatable deformation response in cyclic loading. Many numerical, experimental, and analytical studies have been conducted to develop means of predicting their large deformation mechanical and optical responses. See, for example, refs 1−4. A special class of silicone elastomers, called bimodal because of their bimodal molecular weight distribution of starting oligomers, has shown very promising mechanical properties. Experimenters have demonstrated that certain bimodal systems have ultimate strength and toughness values in excess of those exhibited by unimodal specimens of their constituents.[1,5] The anomalously high property values found in particular bimodal compositions are integrally linked to the network structure and its deformation characteristics. The topological features responsible for the synergistic deformation response of certain bimodal compositions have not been identified.

Many researchers have sought to experimentally determine the origins of these enhanced mechanical properties.[4,6−8] Measurements of segmental orientation taken from IR dichroism experiments on various bimodal PDMS specimens in tension suggest the short (long) chains deform less (more) than their counterparts in a unimodal specimen for a given amount of macroscopic deformation.[4,6] Increased toughness is attributed to delays in failure of the much stiffer short chains. Static[7] and dynamic[8] light scattering experiments on bimodal PDMS specimens have suggested that the short chains tend to group together during cross-linking forming a heterogeneous network structure which may affect the network's strength and toughness. The length scale of the heterogeneity according to Soni and Stein[7] was equivalent to the entanglement length.[9] Oikawa[8] reported that the length scale would comprise "many" short chains but did not give a quantitative estimate. Optical birefringence measurements of bimodal PDMS have suggested that a constituent molecular weight

dependent critical concentration of short chains is necessary to produce nonlinear stress−optical behavior at small deformations in an otherwise linear system.[10−12] The occurrence of nonlinear stress−optical behavior has been linked to limiting extensibility of the molecular chains in unimodal networks[3,13] which suggests that in bimodal networks, though a portion of the molecular chains reach limiting extensibility early, network failure is delayed, thereby increasing toughness.

Experimental studies have provided some insights into understanding the responses of long and short chains in bimodal networks. Computational studies seek to determine explicitly the interactions between the long chains and the short chains in the network while adhering to the frameworks derived from experimental observations. Termonia used an ordered, two-dimensional lattice based computer simulation of bimodal network deformation to examine the relationship between differential stretching and enhanced strength and toughness.[14,15] In accordance with Monnerie et al.,[4,6] his work clearly showed differential stretching and load bearing between the two molecular species in the simulated bimodal elastomer network, however, the ultimate strengths and toughnesses of the networks were lower than expected due to a premature assignment of failure of the short chains.

A recent computational investigation used a three-dimensional version[16] of the bond fluctuation model[17] to examine the spatial distribution of the molecular chains in the elastomer system before and after cross-linking. In contrast to previous experimental observations[7,8] Hagn et al.[16] reported that the pair correlation functions of their simulated bimodal systems were spatially homogeneous in the melt and in the final, cross-linked network; i.e., before and after cross-linking, short chains were dispersed evenly throughout their systems. The authors believe the discrepancy is related to the distinction between having a mechanically equilibrated and a kinetically equilibrated cross-linked system.

It is clear from experimental observations that the mechanical response of a bimodal system is dependent

on the system's composition[4,6,10–12] and that optimal bimodal structures exist for strength and toughness enhancement.[1,5] Computational investigations validate some micromechanical ideas suggested by experiment but are limited by the physics on which they are based. Computational searches for optimal structures require a realistic pre-cross-linking arrangement of reactive agents and molecular chains,[2,16,18–20] a representative simulation of the cross-linking event,[2,14,15,18,21] diffusive relaxation[16,17] of the system, and topological assessment.[2,18–20] Computational algorithms must also relate topological results from the simulations to a constitutive formalism in order to measure, at least qualitatively, the extent to which a given bimodal system's structure is optimized for strength and/or toughness. The program NETSIM introduced herein brings together realistic arrangements of the precursor chains, an accurate and efficient representation of the cross-linking event, and a system that is effectively relaxed in a diffusive sense (i.e., all chemical species are evenly distributed throughout the system). NETSIM results also uncover a possible metric of network optimization. Since the information needed to investigate topological structures stems solely from network connectivity, mechanical relaxations are left for future work.

Previous cross-linking simulations are discussed in section 2. The NETSIM algorithm is detailed in section 3. In section 4 the results of convergence studies are reported followed by gel and sol fraction content and gel fraction topology studies for tetrafunctional and trifunctional networks of unimodal and bimodal compositions. Unimodal results are provided for comparison with previous research; bimodal topological studies are presented for the first time. Topological features responsible for enhanced bimodal network properties are identified based on trends in their occurrence and comparison with mechanical property data in the literature. A length scale associated with these features is defined in section 4.4. Concluding remarks are presented in section 5.

2. Cross-Linking Simulations

Previous cross-linking simulations have focused on topological investigations of unimodal systems, kinetic analysis of unimodal and bimodal network structures, and spatial distributions of molecular species within unimodal and bimodal networks; see for example.[2,14,16] Some important contributions and their relevance to this work are discussed below.

A two-dimensional kinetic model for a bimodal elastomer has been introduced by Termonia[15] to address the specific interaction of long and short chains. Termonia's work incorporated a highly efficient on-lattice framework for network generation, used physical entanglements in addition to chemical cross-linking sites, analyzed the partitioning of the deformation of the network, and introduced bimodal constituents for the first time in computational simulations. The lattice arrangement, however, independently associated an end-to-end vector length and a molecular weight between vertexes with the distance between each grid point. This effectively overrode classical assumptions relating chain vector length to molecular weight[24] which may have affected the chain's nonlinear entropic force-stretch law by giving the unperturbed chain an end-to-end distance other than its rms length. To rectify the situation, Termonia adjusted the molecular weights of the chains to fit the rms assumption. To accommodate resulting differences in the unperturbed forces in long and short chains, Termonia assigned "residual" forces to ensure equilibrium at chemical cross-link points in the unperturbed state. The Termonia results provide evidence of differential stretching in the long and short chains and of overall strength increases upon deformation in bimodal systems stressing the need to examine bimodal chain distributions. Network topology was not addressed beyond gel and sol fraction measurements reported to be in agreement with experimental results.[15] Large simulation sizes, 10 000 chains or more, were suggested in order to decrease boundary effects. Termonia's work shows the lattice arrangement, while a highly efficient tool for network generation, would not be robust in generating broad spectrums of molecular weight combinations for general bimodal systems since the lattice itself excludes certain mixture combinations.

A recent computational study of bimodal elastomer networks examined the spatial distribution of short chains in the melt and then again after cross-linking in three dimensions.[16] This Monte Carlo (MC) simulation used an extension of the two-dimensional bond-fluctuation model[17] to determine the kinetically equilibrated arrangement of polymer chains and reactive agents. Simulations using 10^6 MC cycles on systems of roughly 2×10^4 chains were performed in the three-dimensional case to find kinetically relaxed arrangements of the system prior to cross-linking. After relaxation, chain ends were cross-linked on a nearest neighbor basis, and the system was relaxed again. Hagn et al.[16] concluded from analysis of the local averages of pair correlation functions that the short chains are distributed uniformly throughout the system both before and after cross-linking. This result is crucial because it proves that the nearest neighbor cross-linking search does not, by itself, alter the homogeneity of the system. Spatial homogeneity, over a suitable length scale, is a rubric of computational network simulations.[2,14–21] Examination of spatial distributions of bimodal systems after cross-linking, however, should involve analysis of both kinetic equilibrium, as in the bond-fluctuation model, and mechanical equilibrium. The latter consideration may be achieved by including a mechanical relaxation after cross-linking to account for the different constitutive responses of long and short chains affecting the equilibrated length of each once they share a common junction.

Eichinger has reported extensive computational investigations of the cross-linking event in various unimodal systems.[2,18–21] Eichinger's approach utilized a spatially continuous distribution of components inside the reaction box, generation of a data structure containing network connectivity information which could be analyzed using graph theory, and a means of reducing computational size by subdividing the reaction box. Eichinger's work also assumed a Gaussian distribution of end-to-end lengths and phantom behavior of the network chains. In the Eichinger approach, after subdividing the reaction box into smaller subboxes, cross-linking was performed on a nearest neighbor basis between reactive agents in the current subbox and those chain ends in the current or an adjacent subbox until a desired extent of reaction was achieved. However, by disallowing reactive agents in subboxes adjacent to the current one from participating in the nearest neighbor cross-linking search a possible bias in cross-linking was

introduced. This biasing allowed cross-linking *across* the edges of a subbox to occur without first accounting for *internal* cross-linking within the adjacent subbox, thus promoting formation of the gel. In addition, the adjacent subbox was partially depleted of possible cross-link sites before it became the central subbox in a nearest neighbor cross-linking search. Eichinger's method also produced chains with ends dangling outside the reaction box's boundaries. These dangling ends were at an unrealistic disadvantage in the simulated cross-linking event due to their distance from the reactive agents which were restricted to the reaction box. To compensate for this biasing and to minimize boundary effects, a minimum cell size of 5000 chains was suggested,[2,18] and a 10 000 chain cell size was the minimum used. To date Eichinger's work provides the most spatially realistic simulations of cross-linking despite this possible biasing. Gel and sol results were in overall agreement with experimental and theoretical predictions with shorter molecular weights comparing more favorably than longer molecular weights. It must be noted, however, that preferential arrangements in network structure may also affect deformation of the gel, which has not been explicitly investigated. The current NETSIM program is modeled after Eichinger simulations but is modified to remove edge effects and the need for subdivision of the cell as well as to incorporate bimodal molecular chains.

The NETSIM program introduced in this paper provides spatially realistic simulations of the cross-linking process for any molar mixture and molecular weight combination. The program is unique among cross-linking algorithms in that it employs nearest neighbor periodic three-dimensional boundary conditions to remove edge effects. Since the cell is periodic the simulation size may be kept small, roughly 1000 chains, while still approximating a representative volume element. The advent of a small number of chains allows the cross-linking search to be efficiently carried out over the entire simulation cell without introducing biasing from subdivisions. Kinetic relaxation prior to cross-linking is effectively reproduced by generation of an initially spatially homogeneous un-cross-linked system. Cross-linked topologies can be examined without conducting mechanical relaxations using the connectivity information provided by NETSIM. NETSIM is also unique in that it is the first attempt, to the best of the authors' knowledge, at numerically computing gel and sol fractions for bimodal systems vs extents of reaction. Various topological characteristics of bimodal systems vs mole fraction and molecular weight combinations are quantified and used to examine relationships between topology and enhanced strength and toughness.

3. Bimodal Network Generation

3.1. Material Synthesis. The physical process of synthesizing bimodal elastomer was conducted for comparison with simulation predictions. Known masses of the tetrafunctional reactive agent TEOS and difunctional PDMS chains of two distinct molecular weights were stirred together at room temperature to achieve a homogeneous mixture. A catalyst (tin(II) 2-ethylhexanoate) was added and again the mixture was stirred. The sample was allowed to cure for 2 weeks at room temperature. The sol fraction was extracted by swelling the sample in solvent (THF) and then allowing the solvent to evaporate.

The cross-linked material left after extraction of the sol represented well over 80% of the total mass. It is termed the gel fraction, or gel. Material removed during extraction that did not form cross-links with any portion of the gel is considered the sol. The sol is, essentially, not mechanically active in the cross-linked elastomer network. Portions of the gel, such as dangling chain ends or loops, are traditionally considered mechanically inactive defects. Characterization of the gel network is difficult thus accurate prediction of the sol fraction is relied upon for comparing results from NETSIM to experimental results and to other network formation programs. Determining the sol fraction is also critical to establishing an expected extent of reaction, as discussed in sections 3.2 and 4. Determination of the network's defect population is still important because defects, even when not contributing directly to mechanical properties, contribute to chain density, mass, and other measures used to characterize networks.

3.2. Simulation Algorithm. A mixture of N_0 difunctional end-linking prepolymer chains of two distinct molecular weights, M_s and M_l, were reacted with initially f-functional cross-linking-agents in a virtual reaction box. The length of one side of the box, L, is given by

$$L = \left(\frac{n_0 M_0}{\bar{\rho} A_{vg}}\right)^{1/3} \tag{1}$$

where A_{vg} is Avogadro's number, $\bar{\rho}$ is the mole-weighted average density of the long chains and short chains, M_0 is the molecular weight of a single monomeric unit and n_0 is the number of monomeric units in the system. n_0 is given by

$$n_0 = \frac{N_s M_s + N_l M_l}{M_0} \tag{2}$$

where N_s and N_l are the final numbers of long chains and short chains, respectively. During chain generation, the ith chain is designated either long or short following the rule: If $\zeta_i \leq m'_s$ then $M_i = M_s$ else $M_i = M_l$, where ζ_i is a random number [0,1] generated for the ith chain and the currently *required* molar concentration of short chains, m'_s, is given by

$$m'_s = \frac{m_s N_0 - \bar{N}_s}{N_0 - (\bar{N}_s + \bar{N}_l)} \tag{3}$$

where m_s is the desired final mole fraction of short chain material in the system and $\bar{N}_s$ and $\bar{N}_l$ are the current numbers of long and short chains in the system, respectively. The number of f-functional reactive agents, g, is given by
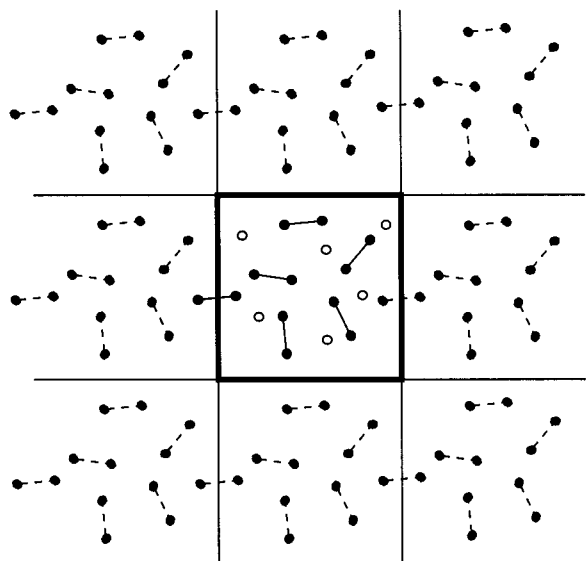
$$g = \frac{2N_0}{f} \chi \tag{4}$$

where χ measures the relative stoichiometry of the system. The initial end-to-end distance of a chain is given by its rms length

$$R_i = \sqrt{C_\infty \frac{M_i}{M_0} d^2} \tag{5}$$

where C_∞ is the characteristic ratio,[22] M_i is the molec-

Figure 1. Image and basis chains and agents in two-dimensional periodic simulation. Agents are denoted by open circles, chain ends by filled circles, basis chains by solid lines, and image chains by dashed lines.

ular weight of the chain in question ($i = $ l, s), and d is the length of a monomeric unit. Our primary investigation involves differences in the characteristics of long and short chains that have initial lengths roughly an order of magnitude apart. For these analyses, a distribution of initial lengths for the individual long and short chains about their respective means is unnecessary. The largest short chain molecular weight studied is less than one-seventh the entanglement molecular weight. The short chains constitute an overwhelming majority of the system in the mixture regime of interest. Therefore, the effects of entanglements can be assumed to be small and will be neglected in the analysis.

Simulated cross-linking employed a nearest neighbor approach similar to work by Eichinger and others and used successfully in the simulated cross-linkings of several different unimodal elastomer chain topologies.[2,16−21] Internal biasing in cross-linking was avoided by using the entire periodic simulation cell in the nearest neighbor search algorithm. Periodic boundaries also removed all edge effects. Network cross-linking proceeded by joining chain end/reactive agent pairs in order of increasing separation distance, r. The following flowchart describes the steps in the simulation process.

- (I) Generate reaction box with edge length L.
- (II) Place g reactive agents randomly within box.
- (III) Chain placement: repeat for $k = 1 \rightarrow N_0$
— (i) Place kth chain's first endpoint randomly within box.
— (ii) Place kth chain's second endpoint randomly a distance R_i ($i = $ l,s) from first endpoint.
- (IV) Cross-linking
— (i) Calculate and store separation distances, r_{ij} between agents, $i = 1 \rightarrow g$, and chain ends, $j = 1 \rightarrow 2 N_0$.
— (ii) Sort r_{ij} values in increasing order.
— (iii) Join agent-chain end pairs in order of increasing r_{ij}. Record current extent of reaction, e_{ij}.
— (iv) Repeat step IV-iii until $e_{ij} = e$.
- (V) Generate network connectivity list at desired e_{ij} values. Make sol/gel calculations.

The effect of periodic boundaries on cross-linking can best be seen in two dimensions by Figure 1, in which each chain is assumed to have a basis inside the reaction box and images in each quadrant surrounding the reaction box. The basis representation of each reactive agent also exists inside the reaction box. Images of the agents are unnecessary. The distance, r, between an agent and a given chain end is the smallest of the distances between the agent and each image of the chain end (including its basis); the least distance of nine possibilities in the two-dimensional case. For the three-dimensional case 26 images and 27 possible r values exist for each chain end/agent combination.

Cross-linking between a chain end and a reactive agent occurred if (1) the prospective agent had an available functionality less than the maximum, f, (2) the chain end was unreacted, and (3) the extent of reaction was currently less than the set reaction extent parameter, e. Upon cross-linking, the basis chain end and all of its images were considered reacted.

During cross-linking a matrix containing agent to agent connectivity was generated. Each agent entry contained information about the molecular weight of chains attached to it. A separate set of programs, including the spanning tree algorithm SPANFO,[23] was invoked to determine the connected components (the gel) and to enumerate the long and short topologies. In general, one large particle formed during the cross-linking leaving the remaining components as the sol. In the extraction phase all chains which were not part of the gel were algorithmically removed while defects and sol fraction were calculated.

4. Results

Three-dimensional simulations of endlinking PDMS starting oligomers and initially trifunctional or tetrafunctional agents were examined. In the following passages all reactive agents are described by their initial, not available, functionality. For example, a reactive agent which has four possible reactive sites is termed tetrafunctional whether one, two, three our all four of those reactive positions are available. Initial simulations were performed on an HP 9000/735/B workstation. Later simulations were performed on an HP 9000/778/B180L workstation. Results given are the averages of five runs. Values of the parameters were $M_0 = 37$ g/mol, $C_\infty = 6.4$, $\bar\rho = 0.97$ g/cm^3, $d = 1.64$ Å.[2,18,24]
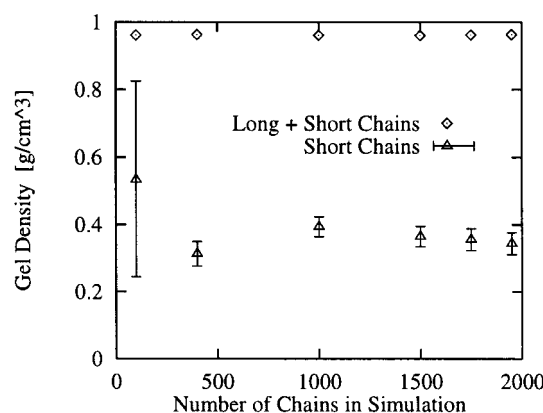
4.1. Convergence Study. Convergence studies were performed on bimodal, tetrafunctional systems with $m_s = 0.97$, $M_s = 400$, $M_l = 21500$, $\chi = 1$, $\bar\rho = 0.97$ g/cm^3 and $e = 1.00$.

Figure 2 shows the percent of connections made by image chains—chains that exit and re-enter the simulation cell—vs the number of chains in the simulation. Error bars denote the standard deviation from the mean. In Figure 2, the number of reentrant connections drops as the number of chains in the simulation cell increases. At roughly 1000 chains, the percentage of connections from reentrant chains has reached its asymptotic value of 19%. This indicates that the density of chains crossing the periodic boundary has reached its limiting value and that the effect of the nearest neighbor boundaries has plateaued.

Figure 3 shows the total gel weight per unit volume and short chain gel weight per unit volume vs the number of chains in the simulation. Error bars in the short chain gel weight per unit volume data denote the standard deviation from the mean. The total gel weight per unit volume data have standard deviations of less
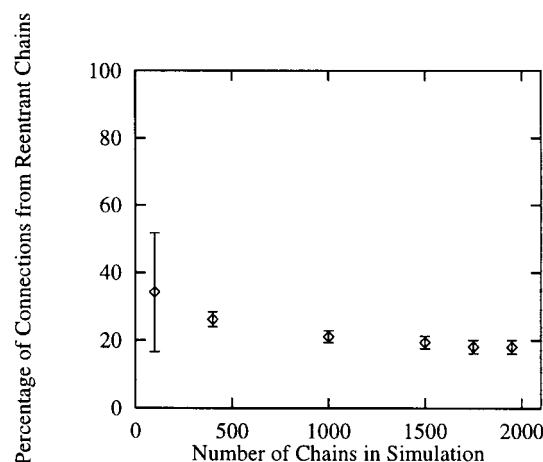
Figure 2. Convergence study of the percentage of reentrant chains vs cell size for a bimodal system, $M_s = 400$ and $M_l = 21\,500$, and tetrafunctional reactive agents.

Figure 3. Convergence study of the gel fraction per unit volume vs cell size for a bimodal system, $M_s = 400$ and $M_l = 21\,500$, and tetrafunctional agents.

Table 1. Composition of Unimodal Systems Studied

system ID	agent functionality	mol wt
1850	4	1850
45000	4	45000

than 0.01 (error bars have been omitted for clarity). At roughly 400 chains the gel weights have reached values consistent with those of much larger cell sizes. Figures 2 and 3 together indicate that at 1000 chains the cell has converged to a representative volume element for this model in terms of boundary effects, total gel content and structure, and short chain gel content.

The simulation algorithm yields molar mixtures accurate to the extent allowed by the number of chains in the simulation cell; eg. a four chain cell may only accurately represent 0, 25, 50, 75, and 100% molar concentration of short chains. To ensure the proper mole fraction mixtures to three significant figures, 1000 chains were necessary. All following simulations were carried out on cells of 1000 chains. As previously noted, all data reported are the averages of five runs. All error bars denote standard deviations of those samples about their respective mean values.

4.2. Tetrafunctional and Trifunctional Unimodal Simulations. Network cross-linking simulations were performed for the unimodal systems given in Table 1. The sol fractions for the systems in Table 1 were computed vs extent of reaction using NETSIM and the results were compared to the numerical results gener-
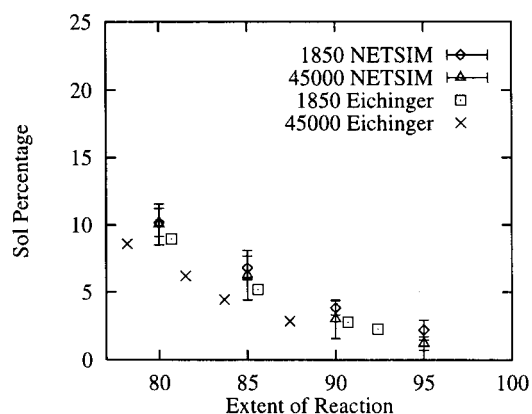
Figure 4. Sol fraction vs extent of reaction for various molecular weights in tetrafunctional.
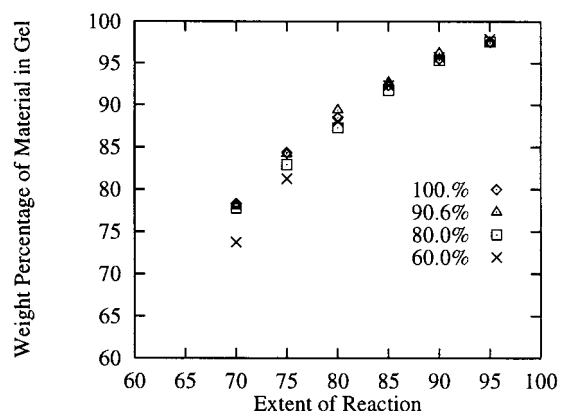
Table 2. Composition of Simulations Corresponding to Experimental Data

system ID	$M_s - M_l$ combination	molar short chain content [%]					
460	21300 − 460	99.6	98.3	97.0	95.4	92.4	90.6
660	21300 − 660	99.7	99.4	98.5	97.0	95.1	94.2 90.8
880	21300 − 880	99.4	98.0	97.0	95.0	93.4	90.8
1100	18500 − 1100	100	89.0	83.0	80.0		0.0

ated by Eichinger.[2,18] Figure 4 shows the NETSIM results compared to work by Eichinger for two tetrafunctional systems. The overall results agree quite well although Eichinger's results predict lower sol fractions than those calculated by NETSIM. We believe this to be a consequence of Eichinger's use of subdivisions in the nearest neighbor cross-linking search. If chains within a subdivision of the cell are allowed to react outside their subdivision before allowing chains within the other subdivision to react, the Eichinger algorithm promotes generation of the gel. Accordingly, the effect increases with molecular weight since longer chains penetrate farther and/or more often into adjacent subdivisions. The differences between Eichinger's results and NETSIM decreases with extent of reaction as nearly the entire system becomes part of the gel. Similar results were found for trifunctional systems. [25] In addition, both Eichinger's results and NETSIM showed a distinct increase in sol fraction for trifunctional systems as compared to tetrafunctional systems for a given molecular weight at a given extent of reaction. This increase occurs due to the difference in the density of reactive agents. For a given number of chains, at $\chi = 1$, tetrafunctional systems have 50% fewer reactive agents than trifunctional systems increasing the likelihood of a given reaction in a tetrafunctional system resulting in gel formation.

4.3. Bimodal Results. Network cross-linking simulations were performed on the tetrafunctional bimodal systems given in Table 2. These particular systems were chosen to correspond to materials synthesized and tested by Mark[1,5] for which toughness data are available. Additional simulations were performed on the mole fraction mixtures and molecular weight combinations given in Table 3 to provide a more complete representation of topologies across a larger spectrum of molar concentrations of short chains.

Figure 5 depicts the mass of the gel fraction of the network during cross-linking as a function of the extent of reaction for four short chain concentrations of system 460. Standard deviations of the results ranged from ±4

**Figure 5.** Gel fraction vs extent of reaction for tetrafunctional bimodal system 460.

Table 3. Composition of Simulations Performed for Completeness

system ID	$M_s - M_l$ combination [g/mol]	molar short chain content [%]			
460	21300 − 460	100	85	80	60
660	21300 − 660	100	85	80	60
880	21300 − 880	100	85	80	60
1100	18500 − 1100		70		

wt % at $e = 0.7$ to ±1 wt % at $e = 0.95$. Error bars are omitted for clarity.

Qualitatively, the results show steady increases in gel fraction with extent of reaction. As the extent of reaction reaches 90% the rate of gel formation decreases. The decrease in the rate of gel formation in simulated bimodal systems follows NETSIM's and Eichinger's results on unimodal systems wherein rate of gel formation also decreases beyond extents of reaction approaching 90%. Quantitatively, results documented elsewhere indicate the authors' experimentally determined weight percentage of material in the gel equal to 96.9 wt %, found from synthesis of a 95% (by mole) short chain mixture of a $M_s = 780$, $M_l = 22210$ combination (very similar to systems 660 and 880), would suggest an experimental extent of reaction near $e = 0.95$.[25] This value is in excellent agreement with the literature which reports extents of reaction of $e = 0.95$ for similar materials and synthesis techniques.[2,15] This result provided independent verification of the sol fraction coupled with an extent of reaction, previously unavailable for this type of material. Results of all simulations to follow are carried out to $e = 0.95$.

Figure 6 shows the total gel fraction, calculated from the total mass of the gel, vs molar short chain content for systems 460, 660, and 880 at $e = 0.95$. The percentage of material in the gel stays relatively constant across all molar mixtures for each system. There is also little differentiation among the bimodal systems. In Figure 7 the mass of material that forms single loops in the gel has been removed before calculating the gel fraction. This is important since loops do not actively contribute to the mechanical properties of the network. Figure 7 shows clear delineation among the three bimodal systems. Figure 7 also shows an increase in the gel weight (*sans* loops) with both molar short chain content and molecular weight of the short chains. Figure 7 predicts that as the molar short chain content increases, the amount of mechanically active material will also increase and that as the molecular weight of the short chain material is increased, the mechanically active mass will increase for a given molar mixture.
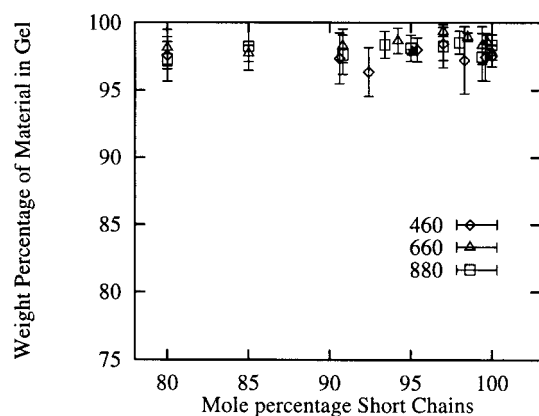
Figure 6. Gel percentage by weight vs molar short chain concentration for bimodal systems 460, 660, and 880.
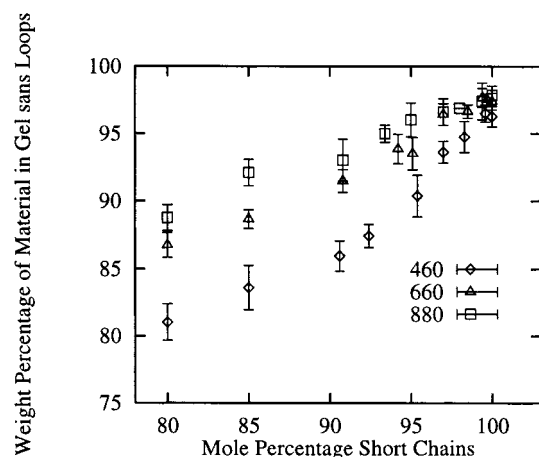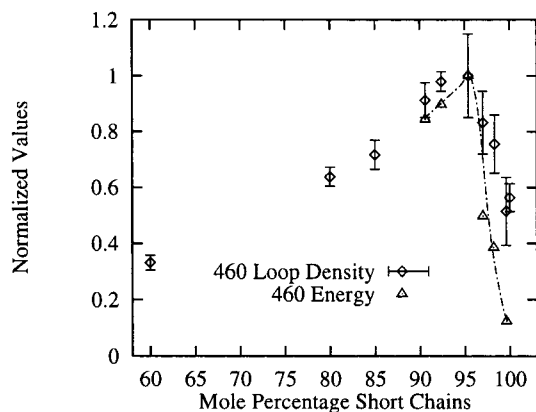

Figure 7. Gel percentage (*sans* loops) by weight vs molar short chain concentration for three bimodal systems.
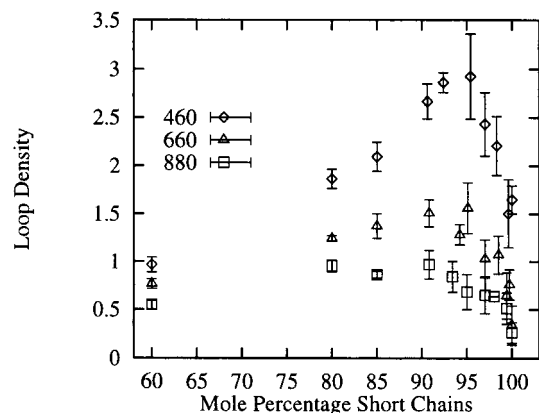

Figure 8. Loop density vs molar short chain content for three bimodal systems.

Figure 8 displays the density of loops in the gel fraction of the material vs the molar short chain content in the three bimodal systems 460, 660, and 880. In each case, loops are formed almost exclusively from the short chains. A statistically insignificant number of long chain loops were found in some simulations. The figure shows a distinct peak in loop density for the bimodal system with the shortest molecular weight, system 460, and broader peaks for the two remaining systems.

Figure 9 shows the values of the loop density and the experimentally determined strain energy at failure,[1,5] each normalized by their maximum values, vs molar short chain content for bimodal system 460. Similar
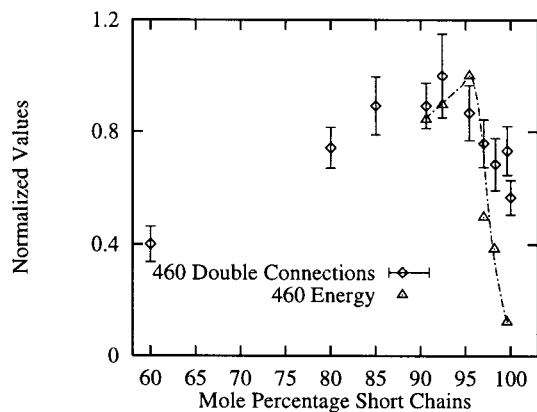
Figure 9. Normalized loop density and normalized strain energy at failure[1,5] vs molar short chain content for bimodal system 460.
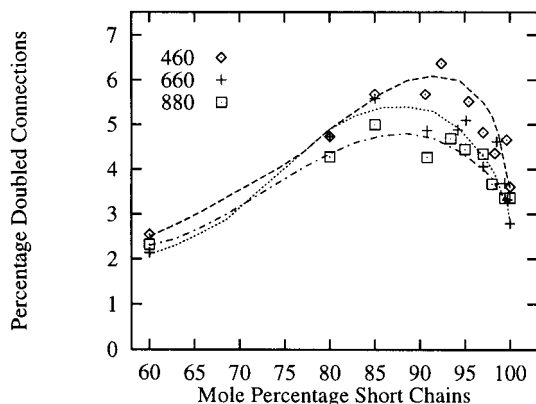
Figure 10. Percent doubled connections in the gel vs molar short chain content for three bimodal systems.

studies where conducted on systems 660, 880, and 1100. Figure 9 clearly indicates a strong correlation between the molar concentrations at which increased loop density occurs in simulations and enhanced toughness is observed experimentally. In fact, the point of maximum loop density corresponds to the point of maximum strain energy at failure for three of the four systems examined. In the case of system 880 the points of maximum strain energy at failure and maximum loop density differ only by the distance between sampling points, 3% in molar short chain content. It is counterintuitive to suspect that an increase in a metric of defect density would correspond to increases in toughness. However, macrocylics (multichain loops) found in computer simulations of sequentially generated interpenetrating networks have been linked to the increases in toughness seen in those systems (though this effect is reportedly due to increased numbers of entanglements).[26] We will demonstrate in section 4.4 a correlation between increases in the density of chains driven to form loops and the number of chains that form network reinforcing structures.

Two tetrafunctional agents in the gel may be connected to each other by at most three molecular chains. A connection is defined as any chain or chains linking two separate reactive agents. The infrequent occurrence of *tripled* connections in simulations is statistically insignificant. A *doubled* connection occurs when pairs of reactive agents are linked to each other by two distinct molecular chains. Figure 10 plots the percentage of doubled connections in the gel vs the molar short chain content for the family of three bimodal systems


Figure 11. Normalized percentage of doubled (short chain) connections in the gel and normalized strain energy at failure[1,5] vs molar short chain content for bimodal system 460.

460, 660, and 880. The percentage of doubled connections is calculated as the number of doubled connections divided by the total number of connections in the network. In Figure 10, error bars are removed for clarity. Combined standard deviations in the reported values for the simulated systems averaged 0.47% doubled connections. Individual standard deviations ranged from $\pm 0.25\%$ doubled connections at 60% molar short chain content for system 660 to $\pm 1.4\%$ doubled connections at 92.4% molar short chain content for system 460. The figure illustrates regions of molar concentration wherein the percentages of doubled connections increase by factors of $1.5-2.5$ from their values in unimodal systems containing the same short chain lengths. Doubled connections are vitally important to the mechanical behavior of the gel since they should be twice as stiff as the connections between singly connected reactive agents. Furthermore, the simulations have shown that these doubled connections are formed exclusively by the much stiffer short chains.

The naturally occurring doubled short chain reinforcement mechanism also correlates well with the molar concentrations at which enhanced toughness properties have been observed. Figure 11 shows the normalized percentages of doubly connected agents and the corresponding normalized strain energies at failure for system 460 vs molar short chain content. The graph shows clear agreement between the molar concentration regions in which enhanced toughness has been observed in experiments and the occurrence of the natural reinforcement mechanism of doubled connections is maximized. Comparable results were found in the three remaining systems.[25]

4.4. Discussion of Topological Results. The enhanced probability of creating doubled connections between agents in the simulation can be viewed as a consequence of the spacing between the reactive agents prior to cross-linking. Figure 12 presents a schematic of two cross-linking scenarios in which two reactive agents arrive at a point during cross-linking where one end of a molecular chain is already affixed to each. The end-to-end vectors of the molecular chains are oriented in the general direction of each other. In Figure 12a the random placement of reactive agents is such that the agents are separated by a distance roughly equivalent to the end-to-end distance of a short chain. In Figure 12b the spacing between reactive agents is much smaller than a short chain's end-to-end distance. The former has an advantage in forming multiple connec-
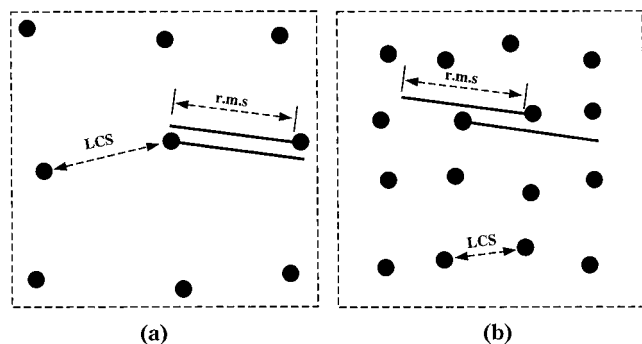
Figure 12. Spacing of reactive agents prior to cross-linking: (a) spacing optimal for producing doubled connections; (b) spacing far from optimal.

tions in the simulations because a nearest neighbor search which extends from one chain's free end will find the other chain's agent (and *vice versa*) whereas in the latter case the two free ends will each find separate agents.

This spacing can be quantified by defining a metric called the *linear cross-link spacing* (LCS)

$$LCS = \left[(M_l - m_s (M_l - M_s)) \frac{f}{A_{vg} b \chi \bar{\rho}} \right]^{1/3} \qquad (6)$$

where b is the functionality of the molecular chains. For the linear PDMS chains examined in the simulations, $b = 2$. LCS computes the cube root of the ratio of the volume of the material to the number of reactive agents present to determine the average linear spacing between the agents. LCS depends solely on the composition of the material. Optimality of the spacing for forming doubled connections is then represented by the dimensionless metric

$$\Omega = \frac{\left[(M_l - m_s (M_l - M_s)) \frac{f}{A_{vg} b \chi \bar{\rho}} \right]^{1/3}}{\left(C_\infty \frac{M_s}{M_0} d^2 \right)^{1/2}} \qquad (7)$$

which is the ratio of the LCS to the short chain rms length, R_s. Unlike LCS, R_s depends on a molecular weight dependent parameter, the characteristic ratio, C_∞, which is determined experimentally under theta conditions.[22] The experimentally determined value is valid only for very long molecular weights. The expression in eq 7 decreases monotonically with increasing m_s, M_s, b, χ, $\bar{\rho}$, d, and C_∞; it increases monotonically as M_l and f increase. This follows physical intuition in that the former set of parameters increase the packing of the molecular chains; the most obvious example of which is $\bar{\rho}$. Equation 7 is maximized when $m_s = 0$ corresponding to a dispersed long chain system; Ω is minimized when $m_s = 1$ corresponding to a more densely packed short chain system.

Figure 13 plots the value of Ω at experimentally determined maximum values of failure energy, computationally determined percentage of doubled connections in the gel, and computationally determined gel loop density vs the molecular weight of the short chains for systems 460, 660, 880, and 1100. These particular values are labeled critical since they represent values of the dimensionless metric Ω at which an energy parameter or the incidence of certain topological features is maximized. The figure also shows Ω values for
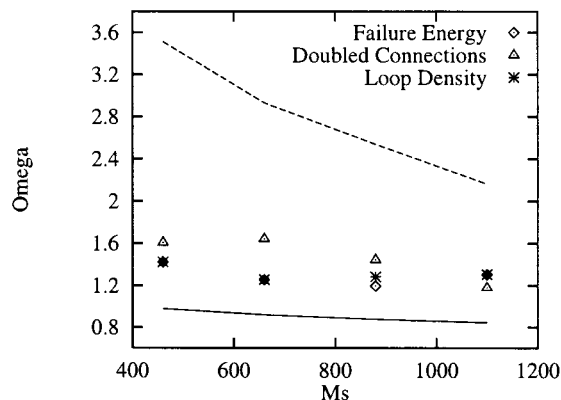
Figure 13. Ω values at maximum incidence of ($\diamond$) failure energy,[1,5] ($\triangle$) doubled connections and ($*$) loop density vs M_s. Solid and dashed lines represent bounding Ω values for unimodal short and nearly unimodal long ($m_s \to 0$) specimens, respectively.

Table 4. Normalized Maximum Strain Energy at Failure for Four Bimodal Systems

system ID	normalized maximum strain energy at failure
460	0.795
660	1.00
880	0.765
1100	0.459

nearly unimodal long compositions, $m_s \to 0$, and unimodal short compositions, $m_s = 1$, with $M_l = 21\,300$ and the M_s values shown. Bounding Ω values for the unimodal cases range from 3.5 to 0.9. Critical Ω values all fall within a narrow band between 1.2 and 1.6. The figure clearly shows how critical values of Ω for loop density follow critical Ω values for strain energy. Whereas previous investigations have focused on determining optimal molar concentrations of short chains in bimodal systems, Figure 13 highlights the advantage of analyzing topological structures and spacing. Each bimodal blend examined demonstrated enhanced strain energy at failure at short chain concentrations that produced the highest loop density. Table 4 lists the experimentally determined maximum strain energies at failure[1,5] for all four bimodal systems normalized by the maximum value which occurs in system 660. In this system, Figure 13 demonstrates that the critical spacing for doubled connections is quite different from the critical spacing for loop density.

The standard deviations in Ω, determined by the sampling point spacing, are equivalent to 1−3 mol % short chains. Though systems 460, 660, and 880 have different long chain molecular weights than those in system 1100, the difference between them is small compared to the smallest difference in short and long chain molecular weights in bimodal systems. All four cases comprise systems wherein the network structure is determined by how short chains and substantially lengthier long chains compete for cross-linking sites. The critical loop densities exhibit a possibly limiting behavior, approaching a value of $\Omega = 1.3$ as M_s increases. This result suggests that as the short chain molecular weight increases, the critical spacing needed for loop formation approaches a limiting value. The doubled connections data depict an overall decrease from $\Omega = 1.6$ to $\Omega = 1.2$ as the short chain molecular weight varies from $M_s = 460$ to $M_s = 1100$. This result suggests that the critical spacing for doubled connec-

tions decreases as the short chain molecular weight increases and would continue to decrease. The overall enhancement of toughness appears to occur for a bimodal blend in which the critical spacing for doubled connections occurs at a concentration of short chains that is quite different than that short chain concentration which maximizes the short chain loop density.

5. Conclusions

The network formation simulation program, NETSIM, provides reliable simulations of the network formation process for endlinking linear polymer chains and *f*-functional reactive agents. The periodic boundaries remove the possibility of errors due to edge effects and reduce the necessary computational size. The smaller simulation cell alleviates the need for subdivision and any possible errors associated with it. Results of unimodal simulations are in agreement with previous investigations; deviations are thought to occur because of biasing in the previous investigations. Results of bimodal simulations show monotonic increases in gel size with extent of reaction. Results also show decreasing populations (by weight) of loops in the gel with increasing short chain molecular weight and increasing molar short chain content. Loops are exclusively formed from short chains. The molar short chain concentrations at which the magnitudes of certain short chain topologies peak, namely the density of loops in the gel and the percentage of doubled connections in the gel, were found to correlate well with the molar concentrations at which enhanced toughness was seen in experiments. Loop density and, to a lesser extent, doubled connections were shown to be clear predictors of enhanced toughness.

Figure 13 in conjunction with eq 7 provides a recipe for generating bimodal samples with increased toughness properties by dictating particular m_s and M_s combinations for the given M_l. Figure 13 suggests that for a given M_s, optimal specimens will have Ω values equal to their critical loop values, Ω_{loop}. m_s may then be determined using eq 7, with $\Omega = \Omega_{loop}$, the given M_s and M_l, and known material parameters. For the systems studied, the optimal M_s is one which provides the largest difference between Ω values for critical loop density and critical doubled connections, Ω_{loop} and Ω_{double}.

The synergy which causes enhanced toughness at certain mixtures in the bimodal systems may be explained as follows. Reductions in the number of mechanically active chains, due to increased loop formation, result in an increase in the strain per network chain. In addition, increased loop formation and increased numbers of doubled connections occur near the same mixtures. The combination creates a reinforced network consisting of a reduced number of chains. The presence of doubled connections is more keenly felt at the mixtures in which the active chain numbers are reduced.

Recent experimental and analytical studies on networks with trimodal distributions have suggested that trimodal systems in which two relatively long components ("long" and "very" long) exist with a short chain component may produce enhancements in material properties beyond those seen in bimodal networks.[27] In contrast, trimodal systems in which two relatively short chain components, named short and very short, exist with a single long chain component will not exhibit toughness properties surpassing those of bimodal or unimodal networks. The difference is said to occur because the chain length distributions of a system with two short chain components resemble simple unimodal networks too closely.[27]

Though they have not been explicitly investigated in this work, the authors believe certain trimodal distributions may show increases in self-reinforcing mechanisms. In the NETSIM model, trimodal distributions would have two distinct optimal spacings for doubled connections that would depend on the lengths of the shortest and middle-length chains. However, a network's propensity for forming doubled connections is dependent on both its LCS and the overabundance of chains near that LCS length. In this sense a trimodal system, dividing its chains among three populations, would dilute the effectiveness of each of its optimal arrangements. On the other hand, the presence of intermediate chain lengths may increase the chances of loop formation which is also a possible factor in the synergistic reinforcement scheme. The issues surrounding trimodal distributions require more thorough investigation.

Efforts are underway to examine the mechanics of the toughening effect. The next step in the analysis involves annealing of the cross-linked structure to examine the rms initial chain length assumption used in rubber elasticity, specifically its applicability to bimodal systems in which the two molecular species obey different force stretch laws and in which multiple connections between reactive agents are important. After annealing is performed, the structure must be deformed to better understand the evolution of the mechanical response in each molecular species and in each topology. Direct comparison of strain energy densities at failure may be made using the simulated deformation studies.

References and Notes

(1) Mark, J. E. *Adv. Polym. Sci.* **1982**, *44*, 1−25.
(2) Eichinger B. E.; Leung, Y. K. *J. Chem. Phys.* **1984**, *80*, 3877−3884.
(3) Arruda, E. M.; Boyce, M. C. *J. Mech. Phys. Solids* **1993**, *41*, 389−412.
(4) Monnerie, L.; Besbes, S.; Ceremelli, I.; Bokobza, L. *Macromolecules* **1995**, *28*, 231−235.
(5) Mark, J. E.; Tang M. Y. *J. Polym. Sci.: Polym. Phys. Ed.* **1984**, *22*, 1849−1855.
(6) Bahar, I.; Erman, B.; Bokobza, L.; Monnerie, L. *Macromolecules* **1995**, *28*, 225−231.
(7) Soni, V. K.; Stein R. S. *Macromolecules* **1990**, *23*, 5257−5265.
(8) Oikawa, H. *Polymer* **1992**, *33*, 1116−1119.
(9) The entanglement molecular weight for PDMS is 8150 g/mol.[15] The entanglement spacing may be found from eq 5.
(10) Galiatsatos, V.; Mark, J. E. *Macromolecules* **1987**, *20*, 2631−2632.

(11) Galiatsatos, V.; Mark, J. E. In *Silicon Based Polymer Science: A Comprehensive Resource*; Zeigler, J. M., Fearon, F. W. G., Eds.; American Chemical Society: Washington, DC, 1990; pp 201−206.

(12) Galiatsatos, V.; Subramanian, P. R. *Makromol. Chem., Macromol. Symp.* **1993**, *76*, 233−240.

(13) Arruda, E. M.; Przybylo, P. A. *Polym. Eng. Sci.* **1995**, *35*, 395−402.

(14) Termonia, Y. *Macromolecules* **1989**, *22*, 3633−3638.

(15) Termonia, Y. *Macromolecules* **1990**, *23*, 1481−1483.

(16) Hagn, C.; Wittkop, M.; Kreitmeier, S.; Trautenberg H. L.; Holzl, T.; Goritz, D. *Polym. Gels Networks* **1997**, *5*, 327−337.

(17) Carmesin, I.; Kremer, K. *Macromolecules* **1988**, *21*, 2819−2823.

(18) Eichinger B. E.; Leung, Y. K. *J. Chem. Phys.* **1984**, *80*, 3885−3891.

(19) Eichinger, B. E.; Shy, L. Y. *Macromolecules* **1986**, *19*, 2787−2793.

(20) Eichinger, B. E.; Galiatsatos, V. *J. Polym. Sci.: Part B: Polym. Phys.* **1988**, *26*, 595−602.

(21) Eichinger B. E. *J. Chem. Phys.* **1981**, *75*, 1963−1979.

(22) Strobl, G. R. *The Physics of Polymers*; Springer-Verlag: New York, 1997.

(23) Nijenhuis, A.; Wilf, H. *Combinatorial Algorithms*; Academic Press: New York, 1975.

(24) Treloar, L. R. G. *The Physics of Rubber Elasticity*; Oxford University Press: Oxford, England, 1975.

(25) Von Lockette, P. R. Ph.D. Thesis, University of Michigan, 1999.

(26) Termonia, Y. *Macromolecules* **1991**, *24*, 1392−1396.

(27) Erman, B.; Mark, J. E. *Macromolecules* **1998**, *31*, 3099−3103.